Membrane electroporation: The absolute rate equation and nanosecond time scale pore creation

Zlatko Vasilkoski, Axel T. Esser, T. R. Gowrishankar, and James C. Weaver
Harvard-MIT Division of Health Sciences and Technology, Massachusetts Institute of Technology, Cambridge, Massachusetts 02139, USA

(Received 2 December 2005; published 3 August 2006; corrected 16 August 2006)

The recent applications of nanosecond, megavolt-per-meter electric field pulses to biological systems show striking cellular and subcellular electric field induced effects and revive the interest in the biophysical mechanism of electroporation. We first show that the absolute rate theory, with experimentally based parameter input, is consistent with membrane pore creation on a nanosecond time scale. Secondly we use a Smoluchowski equation-based model to formulate a self-consistent theoretical approach. The analysis is carried out for a planar cell membrane patch exposed to a 10 ns trapezoidal pulse with 1.5 ns rise and fall times. Results demonstrate reversible supraelectroporation behavior in terms of transmembrane voltage, pore density, membrane conductance, fractional aqueous area, pore distribution, and average pore radius. We further motivate and justify the use of Krassowska's asymptotic electroporation model for analyzing nanosecond pulses, showing that pore creation dominates the electrical response and that pore expansion is a negligible effect on this time scale.

DOI: 10.1103/PhysRevE.74.021904 PACS number(s): 87.10.+e, 87.15.Aa, 87.15.He, 87.50.Rr

I. INTRODUCTION

Nanosecond time scale, megavolt-per-meter electric field pulses have the virtue of causing significant electric field induced effects in the cell interior and organelles which, on longer pulse time scales, are protected by the cell plasma membrane. Indeed, a burst of experimental results have shown granule uptake, DNA fragmentation, calcium release, platelet activation, lipid asymmetry destruction, electrically-induced apoptosis, and tumor self-destruction [1–8]. These observations trigger a renewed interest in the biophysical mechanism of electroporation, and an initial exploration led to the formulation of the supraelectroporation hypothesis [9]. This was followed by a description of microdosimety for a cell model with organelles [10]. A key question in understanding these distinct cellular and intracellular effects, which we want to address in this paper, is whether membrane pores can be created on a nanosecond time scale.

The electroporation hypothesis states that membrane-percolating aqueous pores are created transiently within the phospholipid portion of cell membranes. Electroporation is a universal phenomenon by which cells can be loaded both with small molecules (e.g., anticancer drugs, fluorescent tracers) and large molecules (e.g., proteins and DNA). There is also growing interest in utilizing electroporation to transport drug molecules through multicellular barriers such as solid tumors and the stratum corneum of skin, as the conventional application of electric field pulses of ~ 1 kV/cm to cells and tissue strongly increases ionic and molecular transport through phospholipid-based cell membranes [11–18]. Although some Joule heating always occurs as a secondary effect, in most experiments the associated temperature rise is small, and the main effects are attributed to electrostatic interactions.

To put the present paper into context we briefly note the past development of pore-based theories and models. The initial poration theory was based on homogeneous nucleation of membrane defects and the hypothesis of transient aqueous pores in artificial planar bilayer membranes. This was described in seven back-to-back papers by the Chizmadzhev group, which combined both theoretical analysis and experimental measurements [19–25]. Extensions of the theory can be found in Refs. [26–28]. A pore creation energy barrier that depends on the transmembrane voltage, U_{m}, was independently suggested [29,30], and has been a central part of many electroporation models. A key achievement of the early pore theory is the prediction that the rupture of bilayer membranes is a stochastic process, with a highly nonlinear dependence on U_m. Models based on the Smoluchowski equation (SE) describe the evolution of pore size [19,31], and resolve the occurrence of either reversible or irreversible breakdown as a striking feature of electroporation.

More specifically, an early challenge to theoretical models was to explain the results of experiments that exposed a planar bilayer membrane to short electric pulses of 400 ns [32]. The membrane fate in these experiments was irreversible (rupture) for moderate U_{m}, but reversible for larger U_{m}. The SE-based model demonstrates [33] that relatively few pores are created for $U_{\mathrm{m}} \approx 0.5$V, and the corresponding increase in ionic membrane conductance, G_{m}, is insufficient to discharge the membrane before pores reach a critical size that leads to "runaway pore growth" and membrane destruction. The behavior for larger $U_{\mathrm{m}} \approx 1$ V is in striking contrast. Many created membrane pores lead to reversible electrical breakdown (REB), a high conductance state that protects the membrane, and thus G_{m} may discharge before rupture can occur. An extension of the SE-based model demonstrated that pore dynamics results in an approximate $U_{\mathrm{m}}(t)$ plateau for exponentially decaying pulses, a pore-induced maximum fractional aqueous area of order 0.1%, and the membrane capacitance was essentially unchanged [34]. Intracellular effects caused by nanosecond time scale, extremely large pulses, has led to a further use of SE-based models [35–40]. These recent SE-based modeling results focus on ultrashort pulse behavior of $U_{\mathrm{m}}(t)$ at either or both the plasma membrane and organelle membranes, with an emphasis on irreversible intracellular effects.

The asymptotic model of electroporation was subsequently introduced [41–48]. It is equivalent to a two-state model in which a local membrane region contains either no pore or some number of minimum size pores. It represents a simplified version of the SE-based models, in which only the creation and destruction rates are retained, and changes in $G_m(t)$ are attributed entirely to the addition or slow subtraction of single-size pores. The asymptotic model is particularly useful for describing the electrical response due to ultrashort pulses, as will be shown in this paper.

A basic feature of the SE-based model and the asymptotic model is an absolute rate equation estimate of the pore creation time due to thermal fluctuations and an electrically reduced energy barrier, and also of the pore destruction rate that involves local fluctuations near existing pores. The energy barrier to create a conducting membrane pore, W_p, depends explicitly on local dielectric properties and the local value of U_m. A basic question is whether or not the fluctuating, multimolecular system that is identified with a membrane pore can be plausibly described by such absolute rate estimates, particularly for pulses with a nanosecond time scale.

Molecular dynamics (MD) simulations [49–52] offer the prospect of a more fundamental insight into the process of pore creation and destruction, as well as the transport of ions, molecules or even DNA through membrane pores [53]. Initial results are encouraging, in that the stochastic appearance of hydrophilic transient aqueous pores occurs in those simulations, that the fluctuating pore geometry is qualitatively consistent with the early sketches of a toroidal geometry in which the pore interior surface involves rearranged phospholipid molecules, and that the coupling of MD modeling to time dependent membrane charging is found to be consistent with pore formation on a ~5 ns time scale [40]. However, a present drawback is that fine-grained MD models often require much larger electric fields than those used in experiments, and that U_m values required for pore formation far exceed 1 V.

Coarse-grained models overcome this limitation [40], but by definition involve approximate interactions between the molecules and ions of the system. The present computational limitations on the simulation volume dictate the presence of a small total numbers of ions to represent realistic concentrations of solubilized ions and molecules, but in turn give rise to large fluctuations in transport quantities.

Looking forward, as improved MD results are obtained it should be possible to recast their results in terms of functional local models that can be assigned to spatially distributed models of cell membranes, such as the transport lattice approach to modeling single and multiple cells and their response to electromagnetic stimuli [9,10,54,55]. Both passive interactions (e.g., local models for conductive and dielectric properties of aqueous electrolytes, and cell membranes) and active processes (e.g., local models for resting potential sources, voltage-gated channels, and membrane electroporation) can be assigned to appropriate sites throughout a system model of a cellular system. Such approaches provide modular, multiscale models that can describe electrical, chemical, and thermal behavior simultaneously.

The outline of this paper is as follows. In Sec. II we describe the self-consistent theoretical approach including the equivalent electrical circuit of the system, creation and destruction of membrane pores as well as their dynamics. Based on this theory we analyze experimental data [28,56] in Sec. III and by using these results consider the pore creation on a nanosecond time scale. The supraelectroporation hypothesis is further developed and presented in Sec. IV and a complete set of results for the reversible electrical behavior of the membrane is given for a 10 ns trapezoidal electric field pulse of various strengths.

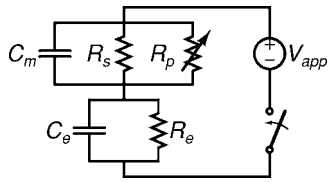

FIG. 1. Equivalent circuit used in our planar cell membrane patch model. We represent the membrane by a R_mC_m element, which includes the time-dependent and nonlinear pore resistance R_p as well as the static membrane resistance R_s. The electrolyte resistance and capacitance are R_e and C_e, respectively, and the applied voltage is V_{app}. The switch is closed for the duration of the applied electric field pulse τ_{pulse}. After the pulse ends the switch is open, thus allowing the membrane to discharge only through the membrane pores and existing channels. U_m is measured across C_m.

II. THEORY AND MODELING METHODS

A. Planar membrane patch model

The polar region of a spherical mammalian cell is represented by a small planar membrane patch. We use a slightly modified version of a previously described bilayer membrane (BLM) model [33,34], in which the membrane response to short electric pulses is analyzed by the electric circuit shown in Fig. 1. In particular, we take the electrolyte dielectric properties into account through the capacitance C_e and note that experimental nanosecond pulses may contain significant frequency components in the gigahertz range. The applied voltage is V_{app}, the electrolyte resistance is R_e, and the membrane is represented by a R_mC_m element, with the membrane capacitance C_m and the membrane resistance R_m. The two parallel contributions to the membrane resistance are due to the static membrane resistance R_s and the time-dependent change in R_p that results from the creation of conducting membrane pores, thus $1/R_m=1/R_s+1/R_p$. For simplicity, no membrane resting potential is used. Passive membrane charging of a spherical cell occurs on a time scale of $\tau_{chg}=r_{cell}C_m(1/2\sigma_{e,ex}+1/\sigma_{e,in})$, which includes the cell radius r_{cell} and external ($\sigma_{e,ex}$) and internal ($\sigma_{e,in}$) electrolyte conductivities. We therefore choose the resistance of the aqueous electrolyte charging pathway to be $R_e=\tau_{chg}/C_m$, and C_e accordingly to assure the bulk electrolyte charging time $R_eC_e=0.6$ ns. In a physiological medium we have $\sigma_{e,ex}\approx\sigma_{e,in}$, but there is a range of values for electrolyte conductivities in different biological systems and experimental protocols. The transmembrane voltage obeys

TABLE I. Membrane and model parameters.

Parameter	Description	Value
r_{cell}	cell radius (μm)	10
d_m	membrane thickness (nm)	5
ϵ_m	membrane relative permittivity (F m^{-1})	$5\epsilon_0$
ϵ_l	(local) lipid relative permittivity (F m^{-1})	$2.1\epsilon_0$
$\epsilon_w=\epsilon_i$	electrolyte relative permittivity (F m^{-1})	$80\epsilon_0$
$C_m=\epsilon_m A_m/d_m$	membrane capacitance (F)	8.8×10^{-14}
ν_0	attempt rate density (s^{-1}m^{-3})	3×10^{36}
r_s	hydrated Cl^- radius (nm)	0.12
σ_e	bulk electrolyte conductivity (S m^{-1})	1.2
T	temperature (K)	293
$r_{p,min}$	minimum pore radius (nm), Ref. [42]	0.8
γ	pore edge energy (J m^{-1}), Ref. [33]	2×10^{-11}
Γ	membrane surface energy (J m^{-2}), Ref. [75]	10^{-5}
n	relative size of pore entrance region, Ref. [59]	0.15
R_s	static membrane resistance (Ω), Ref. [76]	5.6×10^8
D_p	pore diffusion coefficient (m^2 s^{-1}), Ref. [33]	5×10^{-14}

$$(C_m + C_e)\frac{dU_m}{dt} = \begin{cases} C_e\dfrac{dV_{app}}{dt} + \dfrac{V_{app}}{R_e} - U_m\left[G_m(n(r_p,t)) + \dfrac{1}{R_e}\right] & t < \tau_{pulse}, \\ -U_m G_m(n(r_p,t)) & t > \tau_{pulse}, \end{cases} \quad (1)$$

from which the time-dependent transmembrane voltage U_m follows. If the membrane conductance $G_m=G_m^s+G_m^p=1/R_m$ were unchanged during the applied electric field pulse of duration τ_{pulse}, Eq. (1) would have a simple solution in terms of exponential functions. But U_m values on the order of $U_m\sim1$ V have the twofold effect of creating significant numbers of conducting pores and expanding the radius (r_p) of existing pores. The membrane pore conductance $G_m^p(t)$ is thus a function of the pore-size distribution $n(r_p,t)$. The process of pore creation and destruction as well as their time-dependent pore-size distribution will be described by a continuum approach in the following two sections. All values of model parameters are given in Table I.

B. Smoluchowski equation-based models of electroporation

The biophysical mechanisms of electroporation and REB of biological membranes can be described by using the SE [19,31]

$$\frac{\partial n}{\partial t} = \frac{\partial}{\partial r_p}\left[D_p\left(\frac{\partial n}{\partial r_p} + \frac{n}{kT}\frac{\partial \Delta W}{\partial r_p}\right)\right], \quad (2)$$

where $n(r_p,t)dr_p$ is the number of membrane pores between r_p and r_p+dr_p at time t, D_p is the diffusion constant of pores in pore radius space, $\Delta W(r_p,U_m)$ is the pore energy, and kT is the thermal energy. The dynamic pore energy depends on U_m and hence Eq. (2) describes the change in the pore distribution $n(r_p,t)$ due to diffusion and time-dependent drift. As a result the conductance of the membrane, $G_m(n(r_p,t))$, exhibits highly nonlinear time-dependent behavior.

The total pore energy $\Delta W(r_p,U_m)$ is a sum of mechanical and electrical contributions [33,34,57]. The mechanical contribution, $W_m(r_p)$, includes the edge energy per unit length γ and the surface tension Γ of the membrane-water interface. As reference energy we choose the mechanical energy $W_m(r_{p,min})$ at the minimum hydrophilic pore radius $r_{p,min}=0.8$ nm and subtract it to obtain

$$\Delta W_m = 2\pi\gamma(r_p - r_{p,min}) - \frac{\pi\Gamma}{2}(r_p^2 - r_{p,min}^2). \quad (3)$$

The mechanical pore energy determines the equilibrium pore density $n_{eq}(r_p)=n_{eq}(r_{p,min})\exp[-\Delta W_m(r_p)/kT]$, with $n_{eq}(r_{p,min})$ derived from a boundary condition in the next section.

The electric contribution to the pore's energy, ΔW_{el}, which is gained by expanding pores from radius $r_{p,min}$ to r_p, results from the radial displacement of the lipid cylindrical walls of the pore by the aqueous electrolyte. Thus $\Delta W_{el}(r_p,U_m)$ leads to pore expansion at elevated values of U_m. As described previously [27,33,34,57], the electric contribution is

$$\Delta W_{el}(r_p,U_m(t)) = -\frac{\epsilon_0(\epsilon_w-\epsilon_l)\pi}{d_m}U_m^2(t)\int_{r_{p,min}}^{r_p}\eta^2(r)rdr, \quad (4)$$

which is expected to be valid for sufficiently small pores ($r_p<d_m$, see Ref. [46]). Equation (4) includes the membrane thickness d_m, the permittivity of vacuum ϵ_0, and the electrolyte (ϵ_w) and local lipid (ϵ_l) dielectric constant. Furthermore, the function

$$\eta(r_p, r_s, U_m) = \frac{R_{int}(r_p, r_s, U_m)}{R_{int}(r_p, r_s, U_m) + R_{spd}(r_p)} \quad (5)$$

includes the spreading resistance $R_{spd}(r_p)$ and the internal pore resistance $R_{int}(r_p, r_s, U_m)$. The latter contains the steric hindrance $H(r_p, r_s)$ of ions with radius r_s and the partition function $K(r_p, U_m)$ and all together give rise to a non-Ohmic pore conductance. All functions are given in Appendix A.

Having the pore distribution at our disposal we obtain the membrane pore conductance from

$$G_m^p(r_s, U_m, t) = \int \frac{n(r_p, t)}{R_{spd}(r_p) + R_{int}(r_p, r_s, U_m)} dr_p. \quad (6)$$

Electroporation pulses can change the membrane pore conductance over several orders of magnitude, and we use G_m^p self-consistently with Eq. (1) for the equivalent electrical circuit in order to determine the electric behavior of the membrane.

C. Absolute rate equation

Membrane pore formation and destruction initiate and terminate the dynamic membrane pore evolution. In our approach we focus on conducting hydrophilic pores that give rise to a substantial change in membrane pore conductance G_m^p. The formation (destruction) of these membrane states is considered by an absolute rate model describing the crossing of an energetic barrier W_p from (to) nonconducting hydrophobic pores to (from) hydrophilic membrane pores. Furthermore the rate of change in the number of hydrophilic pores $\dot{N}_{p,min}$ is assumed to occur only for pores with minimum hydrophilic pore radius (which corresponds to the local minimum of the hydrophilic pore energy at $U_m = 0$ V, see Ref. [43]), and is given as the difference of creation and destruction rates

$$\dot{N}_{p,min} = \dot{N}_{c,min} - \dot{N}_{d,min}. \quad (7)$$

The absolute rate equation is a well established approach to model homogeneous nucleation of membrane pores that involve multimolecular rearrangements of phospholipids [19,29,33,34,41,58–60]. The Arrhenius-type expression,

$$\dot{N}_{c,min} = A_0 \exp[-W_p/kT], \quad (8)$$

gives the rate of pore creation and involves a prefactor A_0 and the energetic barrier W_p. The energetic barrier W_p to pore formation is reduced by the applied electric field, and we expect W_p to depend on $U_m^2(t)$ if membrane lipid polarization dominates over permanent dipoles. We can thus write $W_p = \delta_c - BU_m^2(t)$. Here δ_c is a fixed energy barrier between the hydrophilic and hydrophobic membrane pore states and B is a model parameter. This approach assumes that pore creation is a stochastic process and can occur anywhere in the membrane. The prefactor A_0 includes the attempt rate density ν_0 (see Appendix B) multiplied by the volume of the phospholipid membrane component, $F_{lip} A_m d_m$, where F_{lip} is the membrane's area fraction of phospholipids and A_m is the membrane area of the membrane patch. Typical values are $F_{lip} \approx 0.5$ for the cell plasma membrane, $F_{lip} \approx 0.25$ for the inner mitochondrial membrane [61], and $F_{lip} = 1$ for the planar patch cell membrane model used here. The creation rate thus reads

$$\dot{N}_{c,min} = \nu_0 A_m d_m \exp\left[\frac{-\delta_c + BU_m^2(t)}{kT}\right]. \quad (9)$$

As in previous models [34] we assume that pore destruction contains an Arrhenius factor as well, but only involves thermal fluctuations in the neighborhood of a pore within a volume $V_{pore} \approx \pi d_m (r_{p,min} + d_m/2)^2 = 1.7 \times 10^{-25}$ m^3. Then the destruction rate is

$$\dot{N}_{d,min} = n(r_{p,min}, t)\chi \exp[-\delta_d/kT], \quad (10)$$

where $N_{p,min}(t) = n(r_{p,min}, t)dr$ is the number of pores at the minimum pore radius, the prefactor χ has the unit of length over time, and δ_d is the energetic barrier for pore destruction. In the case of rapid membrane discharge, U_m has returned to the prepulse value at the experimentally observed pore lifetimes (milliseconds or orders of magnitude longer). This leads to a U_m-independent destruction rate.

The equilibrium state at zero transmembrane voltage exhibits a constant mean value for the number of membrane pores. Thus the creation and destruction rates are equal, and the pore density at $r_{p,min}$ is given by

$$n_{eq}(r_{p,min}) = \frac{A_0}{\chi} \exp[(-\delta_c + \delta_d)/kT]. \quad (11)$$

As a result we can rewrite Eq. (7) as follows:

$$\dot{N}_{p,min} = A_0 e^{-\delta_c/kT}\left[e^{BU_m^2/kT} - \frac{N_{p,min}(t)}{N_{p,min}^{eq}}\right], \quad (12)$$

which is equivalent to the asymptotic electroporation model [41,42] in the limit of a U_m-independent destruction energy barrier δ_d.

III. PORE CREATION TIME SCALES

A. Low applied voltages

Recent studies of conductance fluctuations under low applied voltages by Melikov *et al.* [28] measure the creation time of a single membrane pore. The appearance of one pore is a minimal electroporation event with a small change in membrane conductance on the order of 400 pS [28]. We believe that this experiment provides the simplest method to adjust basic membrane parameters in our theory. Other previous approaches [59] analyzed membrane current data to adjust model parameters, which add another set of assumptions for the pore conductivity (see Appendix A). Melikov's results are displayed in Figs. 2 and 3, which show the creation time for a single membrane pore, t_{lag}, as a function of U_m and applied voltage V_{app}, respectively. In their measurements, the pore creation time scale is on the order of seconds and hence significantly larger than the membrane charging time, $t_{lag} \gg \tau_{chg}$. Then U_m is essentially the applied voltage V_{app} because $R_m \gg R_e$, and the integrated creation rate for the appearance of one membrane pore yields

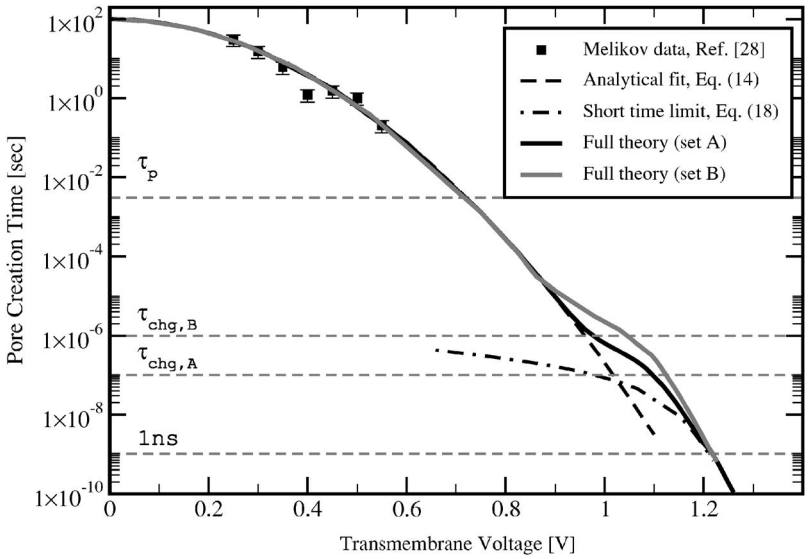

FIG. 2. Mean creation time for a single pore in the planar patch model as function of transmembrane voltage. The Melikov data are fitted according to Eq. (14), and the parameters are subsequently used to evaluate t_{lag} of the absolute rate equation model. The two sets of membrane charging times correspond to (A): Frey's experiment on Jurkat cells ($\tau_{chg,A}=0.1$ μs), and (B): Hibino's experiment on sea urchin eggs ($\tau_{chg,B}=1.0$ μs). The microsecond time scale is reached at about $U_m \approx 1$V with a strong dependence on the charging time constant. The nanosecond pore creation time scale is reached at about $U_m \approx 1.2$ V, and agrees in this regime with the short-time limit represented by Eq. (18). The influence of the pulse rise time is insignificant for the actual value of U_m at which the first membrane pore occurs. Pores can be created at any of the given U_m values, and there appears to be no threshold for electroporation. However, each U_m value corresponds to a particular time scale above which electroporation occurs.

$$1 = \int_0^{t_{lag}} A_0 \exp\left[\frac{-\delta_c + BV_{app}^2}{kT}\right] dt = A_0 \exp\left[\frac{-\delta_c + BV_{app}^2}{kT}\right] t_{lag}. \quad (13)$$

From Eq. (13) we have on a logarithmic scale

$$\ln(t_{lag}) = -\frac{BV_{app}^2}{kT} - \ln(A_0 e^{-\delta_c/kT}). \quad (14)$$

This is a quadratic dependence of the logarithmic time lag on the critical voltage $U_m^c = V_{app}$ at which the first membrane pore appears. A χ^2 fit to the experimental data is shown in Fig. 2 and yields $A_0 \exp(-\delta_c/kT) = 10^{-2}$ s^{-1} and $B = 20\ kT$ V^{-2}. The value of the spontaneous creation rate depends on the membrane area in Melikov's experiment ($A_m = 10$ μm^2). This gives a creation rate density of $A_0/A_m \exp(-\delta_c/kT) = 10^9$ s^{-1} m^{-2}.

We can use these results to map out some relevant information about the free-energy membrane pore landscape. From the definition of A_0 in Eq. (9), the attempt rate density ν_0 in Eq. (B1), and the experimentally based parameter for $\dot{N}_{c,min}$ we can deduce the fixed creation energy barrier to be $\delta_c = 44\ kT$. Given that this value appears in the literature

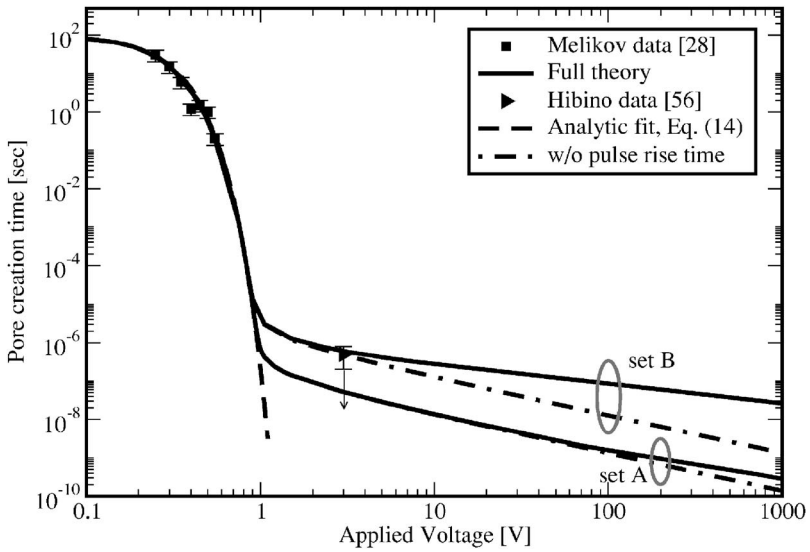

FIG. 3. Mean creation time for a single pore in the planar patch model as function of the applied voltage. Parameters are chosen to represent a mammalian cell such as in Frey's experiment (set A, $\tau_{chg}=0.1$ μs, $\tau_{rise}=5$ ns), and Hibino's experiment on sea urchin eggs (set B, $\tau_{chg}=1$ μs, $\tau_{rise}=0.3$ μs). The Hibino data point must be interpreted as an upper time limit (with error bars corresponding to the temporal resolution) for the onset of poration, which is indicated by a downward pointing arrow. The charging time τ_{chg} and the pulse rise time τ_{rise} both cause an increase in the value of the applied voltage necessary to obtain single pore formation at a given t_{lag}.

TABLE II. Model parameters based on the Melikov experiment.

Model Parameters	Description	Value
A_m	membrane area (m^2)	10×10^{-12}
$N_{p,min}^{eq}/A_m$	equilibrium pore density (m^{-2})	3×10^{6}
δ_c	fixed creation energy barrier (kT)	44
δ_d	fixed destruction energy barrier (kT)	19
$A_0/A_m \exp(-\delta_c/kT)$	pore creation rate density (s^{-1} m^{-2})	1×10^{9}
B	parameter in Eq. (9) (kT V^{-2})	20
τ_p	mean pore lifetime (s)	3×10^{-3}

[42–44,59] and is inferred from conductivity measurements on not exactly the same biological system, we derive some confidence in this basic parameter for membrane electroporation. Considering the mechanical energy of a minimum size pore $W_m(r_{p,min})=25\ kT$, we can also estimate the energy barrier for pore destruction as $\delta_d=\delta_c-W_m(r_{p,min})=19\ kT$.

Another experimental result of Melikov *et al.* [28] is the mean pore lifetime of $\tau_p\approx3$ ms. We use this value to determine the equilibrium pore number $N_{p,min}^{eq}$ in Eq. (12) and have

$$N_{p,min}^{eq}=\tau_p A_0 \exp[-\delta_c/kT]. \tag{15}$$

We thus find Melikov's membrane patch to have $N_{p,min}^{eq}=3\times10^{-5}$ pores with minimum radius at $U_m=0$ V, which corresponds to a minimum size pore density of $N_{p,min}^{eq}/A_m=3.3\times10^{6}$ m^{-2}. This is a time-averaged value. Only occasionally does a pore appear via spontaneous fluctuations and then vanishes according to the mean pore lifetime τ_p. The number of transported ions and molecules through this small number of equilibrium pores can be neglected. The experimentally determined parameters of our model are shown in Table II. This sets the basis for the consideration of pore formation time scales due to stronger and shorter electrical pulses in the remainder of this paper.

B. Strong nanosecond electric field pulses

Nanosecond, megavolt-per-meter electric field pulses achieve a variety of cellular and intracellular effects such as calcium activation, DNA laddering, lipid asymmetry destruction, and arguably the most important to date, electrically-induced apoptosis [2–7]. A key question in understanding the biophysical and biochemical mechanisms which lead to these effects is whether membrane pores can be created on a nanosecond time scale.

For the strong applied electric fields under consideration, the first membrane pore appears during the membrane charging process. Let us first consider a rectangular pulse for which an approximate expression for the time dependence of U_m is

$$U_m(t)=V_{app}(1-e^{-t/\tau_{chg}}). \tag{16}$$

Equation (16) is a simple expression to gain some further insights, and agrees with the exact but lengthy rectangular pulse solution, given in Ref. [62], within 2% error. We numerically integrate

$$1=A_0 \exp(-\delta_c/kT)\int_0^{t_{lag}} e^{BU_m^2(t)/kT}dt, \tag{17}$$

to obtain the creation time t_{lag} for the first membrane pore. The result in Fig. 2 shows a deviation from the result of Eq. (14), which sets in as the membrane charging time τ_{chg} is approached. Two sets of systems are considered. Set A is the mammalian cell discussed in Sec. II A with a charging time constant of $\tau_{chg}=0.1$ μs, and is related to the very recent set of voltage-imaging experiments by Frey *et al.* [63] on Jurkat cells. Set B corresponds to the sea urchin eggs experiments discussed by Hibino *et al.* [56], which have $\tau_{chg}=1$ μs. For even shorter time scales than τ_{chg} there appears an offset, a lengthening of the pore creation time as a consequence of membrane charging delay. As such, the pore creation time for $t_{lag}<\tau_{chg}$ appears to depend on the external and internal electrolyte conductivities, whereas in the regime of $t_{lag}>\tau_{chg}$ (such as in Melikov's experiments) the pore creation time does not. As presented in Fig. 2, the well-known U_m value of about 1 V for electroporation corresponds to a microsecond pore formation time scale, as indeed inferred by Hibino's data [56]. However, there appears to be no threshold for electroporation, as pores can be formed for any U_m value given in Fig. 2. What is decisive for the experimental outcome though is the time scale over which electroporation occurs.

The short-time limit of $t\ll\tau_{chg}$ in Eq. (16), for which U_m has a linear dependence on time as $U_m(t)=V_{app}t/\tau_{chg}$, can be made explicit. Performing the integration in Eq. (17) we derive the condition

$$1=A_0 \exp(-\delta_c/kT)\frac{\sqrt{\pi kT}\tau_{chg}}{2\sqrt{B}V_{app}}\mathrm{erfi}\left(\frac{\sqrt{B}V_{app}}{\sqrt{kT}\tau_{chg}}t_{lag}\right), \tag{18}$$

with the complex error function erfi(x)=erf(ix)/i. Equation (18) represents the short-time limit and is shown in Fig. 2 to be reached by the full numerical solution at $t_{lag}\approx10$ ns. We suggest here that the microsecond time scale at the conventional $U_m\approx1$ V is not the limit yet for the pore creation time scale, as the nanosecond time scale can be reached at a transmembrane voltage of about $U_m\approx1.2$ V.

C. Influence of the pulse rise times

The characteristic rise (τ_{rise}) and fall (τ_{fall}) times of an experimental pulse may have an additional influence on the creation time of membrane pores. We consider an idealized trapezoidal pulse [62] that results in a time-dependent $U_m(t)$ according to

$$U_m(t) = U_{m,t}(t) - U_{m,t}(t - \tau_{rise}),$$

$$U_{m,t}(t) = V_{app}\left[K_1 \frac{t}{\tau_{rise}} + K_2(1 - e^{-t/\tau_1}) + K_3(1 - e^{-t/\tau_2})\right]. \tag{19}$$

Explicit expression for the functions K_1, K_2, K_3, and the membrane charging time τ_1 and the bulk electrolyte charging time τ_2 are given in Appendix C. By using Eq. (19) we readily calculate t_{lag} from Eq. (17). Figure 3 shows the pore creation time as function of the applied voltage $V_{app}=E_{app}r_{cell}$ without the influence of the pulse rise time according to Eq. (16) and including the rise time given by the $U_m(t)$ dependence in Eq. (19). The overall effect of the pulse rise time is to further increase the value of the applied voltage necessary to obtain the first membrane pore at a given t_{lag}.

Other previous experimental results found pore formation in the microsecond range for an estimated transmembrane voltage of $U_m \approx 1$ V, which agrees with the relevant range in Fig. 2 for set B. More specifically, Hibino *et al.* [56] applied a 400 V/cm pulse on sea urchin eggs and found initial membrane poration to occur as early as 0.5 μs, their earliest measurement. We find the measured limit on the pore formation time to be consistent with the prediction of the absolute rate equation, (see Fig. 3). Hibino's experiment though must be regarded as an upper time limit for pore formation as earlier times cannot be ruled out. We do not attempt to translate V_{app} in Hibino's voltage, at which initial electroporation appears, into a corresponding U_m as the error bars would be quite substantial.

IV. SUPRAELECTROPORATION

A complete electrical characterization of a cell membrane response to nanosecond, megavolt-per-meter pulses exhibits reversible supraelectroporation features. In particular, Figs. 4(a)–4(f) show the transmembrane voltage, the total pore number, the membrane conductance, the pore distribution, and average pore radius, and the fractional aqueous area for a 10 ns trapezoidal pulse (7 ns wide flat top, rise and fall times of 1.5 ns) for various electric field strengths. The transmembrane voltage at a field strength of 100 kV/cm and 50 kV/cm shows a REB peak at $U_m \approx 1.4$ V, at which a huge burst of $N_p=10^6$ membrane pores have been created within A_m. A colossal increase of membrane conductance G_m by over ten orders of magnitude is the consequence. The hallmark of supraelectroporation is the order of magnitude of membrane pores [10]. 10^3–10^4 more pores are created within A_m than in conventional electroporation protocols, which for mammalian cells involves electrical pulses of 10^2 to 10^3 V/cm and durations of 100 μs to 50 ms. Supraelectroporation is expected to be cell-size independent [9] and results in the appearance of substantially increased aqueous fractional areas of up to 25% for the highest field strength used. This result clearly suggests, that for even higher field strengths the present electroporation model breaks down and needs to be reconsidered. The second hallmark of supraelectroporation is the size of the membrane pores. As seen in Fig. 4(e), these pores are mainly minimum sized, as the electric field pulse is so short that pores have insufficient time to expand. The consequences for transport are significant, as only small ions and molecules are able to pass through the membrane pores, avoiding the release of bigger molecules and biologically active compounds such as DNA and proteins and thus preventing prompt necrosis. Also traditional electroporation biomarkers such as propidium iodide are inhibited from crossing the plasma membrane through the minimum sized pores. This does not rule out secondary transport processes such as endocytosis by a stimulated cell.

These findings support the use of Krassowska's asymptotic electroporation model [41,42], which can be rederived in our approach in the case of negligible pore expansion. This statement and its relation to the pore radius diffusion constant in the SE are further developed in Appendix D. A third hallmark of supraelectroporation, which we mention in passing and is demonstrated elsewhere [10,64] relates to significant current and field redistribution. Supraelectroporation is pervasive, occurring over the entire plasma membrane [9], and even in subcellular membranes such as the nucleus [10] and the mitochondria, and as such is expected to play a decisive role in the induction of apoptosis by nanosecond electric field pulses.

As shown in Fig. 4(a), the subthreshold 10 ns pulses with a field strength of 1 and 10 kV/cm are not able to cause REB of the membrane, and the pore number and membrane conductance is changed insignificantly. However, as the membrane discharge takes longer for the lower field strengths, transport in cells may then become dominated by voltage-gated channels at supraphysiological voltages. This is a related area of research in which relatively little is known, but electrical denaturation of membrane proteins has been experimentally demonstrated [65,66].

V. CONCLUSIONS

The absolute rate equation describes the formation of membrane pores over a wide range of time scales. We used Melikov's data at low applied voltages [28] to specify the parameters of the absolute rate equation within the regime of seconds. We extrapolate this theory then to higher applied voltages and shorter time scales. By taking into account the membrane charging time constant and the pulse rise time we find consistency with Hibino's [56] set of data in the microsecond regime, and a consistence with membrane pore formation on a nanosecond time scale for extremely high electric field strengths. In light of relatively little quantitative experimental data in the microsecond regime, we believe a reconsideration of this conventional electroporation regime with the now available superior time-resolution dyes could

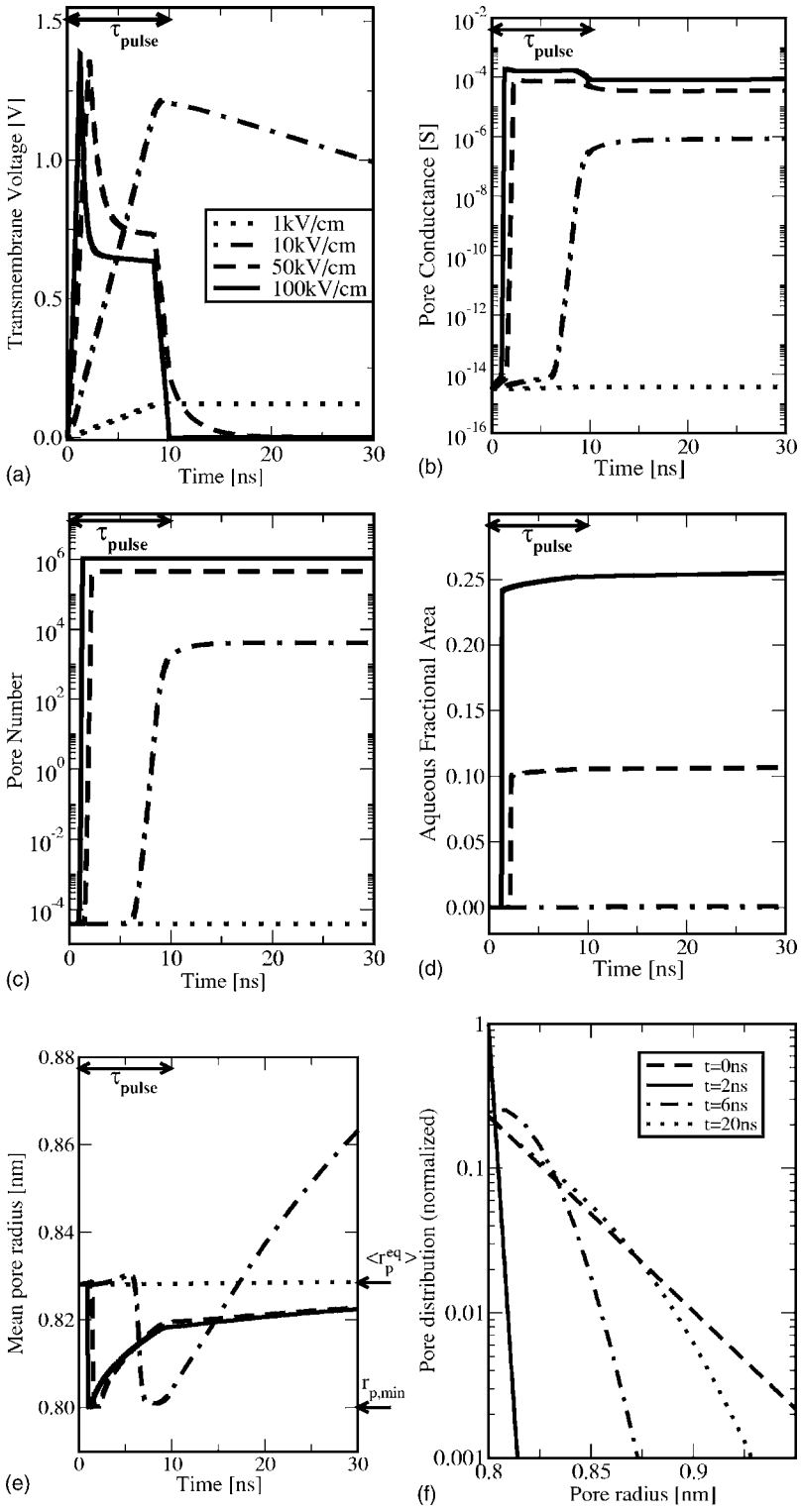

FIG. 4. SE-model for a 10 ns trapezoidal pulse for electric field strengths of 1 kV/cm (dotted line), 10 kV/cm (dotted-dashed line), 50 kV/cm (dashed line), and 100 kV/cm (straight line): (a) U_m shows REB for the two highest field strengths, which creates enough conducting pores to rapidly bring U_m down to an approximate plateau. The 10 kV/cm pulse charges U_m up to an elevated value of $U_m = 1.2$ V, but the time scale is not fast enough for REB. In general, the membrane discharge takes longer for lower applied field strengths. (b) Total pore conductance as function of time, which changes over 10 orders of magnitude for the highest field strength. (c) Time-dependent number of pores on A_m, which reflects the reduction of pore creation time with increasing field strength. The total pore number within the area A_m correlates with a maximum aqueous fractional area of 25% for the highest applied field strength, and is shown in (d). The time-dependent mean pore radius shown in panel (e) demonstrates that these pores are primarily minimum sized pores. Note that the mean pore radius starts at a prepulse equilibrium value $\langle r_p^{eq} \rangle = 0.83$ nm, larger than the minimum pore size $r_{p,min}$. During the nanosecond pulse, many pores with $r_{p,min}$ are created, which are expanded only slightly within the course of the pulse, and then pore destruction brings the pore distribution and the mean pore radius back to equilibrium. The mean pore radius for the 10 kV/cm pulse, however, increases even after the pulse ends because of the slow membrane discharge and the corresponding elevated values of U_m. Panel (f) shows the (normalized) pore distribution for the 100 kV/cm pulse and demonstrates the change from the equilibrium distribution at $t=0$ (that determines $\langle r_p^{eq} \rangle$) to a strong peak at the minimum pore size when REB occurs at $t=2$ ns, a small amount of pore expansion during the pulse (around $t=6$ ns), and the relaxation toward equilibrium after the pulse.

yield tremendous progress toward a full quantitative understanding of electroporation.

Modeling based on the SE predicts reversible supraelectroporation behavior of the membrane upon the application of megavolt-per-meter electric field pulses. These pulses can only be used on a nanosecond time scale without causing a significant temperature rise. The thermally limited pulse duration in turn implies rapid rise and fall times. The electrical response of the membrane is characterized through many minimum-sized pores, which give rise to a rapid change of membrane conductance by ten orders of magnitude, as well as rapid discharge of the membrane after the end of the pulse.

ACKNOWLEDGMENTS

We thank P. T. Vernier, P. Tieleman, C. M. Stultz, D. A. Stewart, K. C. Smith, K. Schoenbach, R. Joshi, R. Nuccitelli,

E. Neumann, R. C. Lee, M. A. Gunderson, R. W. Glaser, Y. Chizmadzhev, S. Buescher, M. Bier, and S. Beebe for many valuable discussions, and K. G. Weaver for computer support. This research was supported by NIH Grant No. RO1-GM63857 and an AFOSR/DOD MURI grant on Subcellular Responses to Narrowband and Wideband Radio Frequency Radiation, administered through Old Dominion University.

APPENDIX A: SINGLE PORE CONDUCTANCE

We combine previous models [33,34,59] to obtain the single-pore ionic conductance $g_p(r_p)$ that depends on voltage-dependent partitioning, steric hindrance, and the spreading resistance. Strictly, each ion species s with its hydrated ion radius r_s and valence z_s gives rise to a particular ionic conductance. Thus in general we expect the dependence

$$i_{p,s} = g_p(r_p, r_s, z_s) U_m. \tag{A1}$$

Here we can use Cl^- as a surrogate for all of the three small ion pore conductances g_{p,Cl^-}, g_{p,K^+}, and g_{p,Na^+}, present in typical extra- and intracellular electrolytes. The spreading resistance R_{spd} [67] on both sides of the membrane and the internal pore resistance R_{int} in terms of the dimensionless steric hindrance factor $H(r_p, r_s)$ and the partitioning coefficient $K(r_p, U_m)$ are

$$R_{spd}(r_p) = \frac{1}{2 r_p \sigma_e}, \tag{A2}$$

$$R_{int}(r_p, r_s, U_m) = \frac{d_m}{\sigma_e A_p H(r_p, r_s) K(r_p, U_m)}. \tag{A3}$$

As in previous models [33,34,57] we use Renkin's steric hindrance factor for $H(r_p, r_s)$ [68]:

$$H(r_p, r_s) = \left[1 - \left(\frac{r_s}{r_p}\right)\right]^2 \left[1 - 2.1\left(\frac{r_s}{r_p}\right) + 2.09\left(\frac{r_s}{r_p}\right)^3 - 0.95\left(\frac{r_s}{r_p}\right)^5\right]. \tag{A4}$$

The voltage dependent partitioning coefficient $K(r_p, U_m)$ takes into account the electrostatic energy barrier for an ion to enter a pore. Following Glaser *et al.* [59], we use a U_m-dependent partition coefficient

$$K(r_p, U_m) = \frac{e^{v_m} - 1}{w^- e^{v_m} - w^+}, \tag{A5}$$

that favors ion entry as U_m increases [9,42]. With the monovalent ion charge e we have defined a dimensionless voltage $v_m = eU_m/kT$ and the auxiliary function is

$$w^{\pm} = \frac{w_0 e^{w_0 \pm n v_m} \pm n v_m}{w_0 \pm n v_m}. \tag{A6}$$

Here, n is the relative size of the entrance region of the pore [59] and $w_0(r_p)$ represents the electrostatic Born energy to place an ion in the middle of a finite-size pore divided by the thermal energy. The bulk self-energy of an ion with radius r_s inside the membrane pore is increased due to image charges and was calculated by Parsegian [69,70] for an infinitely long pore. We correct for finite membrane-size effects by carrying out a three-dimensional calculation of the electrostatic energy to place an ion in the center of a pore of given radius. This yields for a membrane of $d_m = 5$ nm:

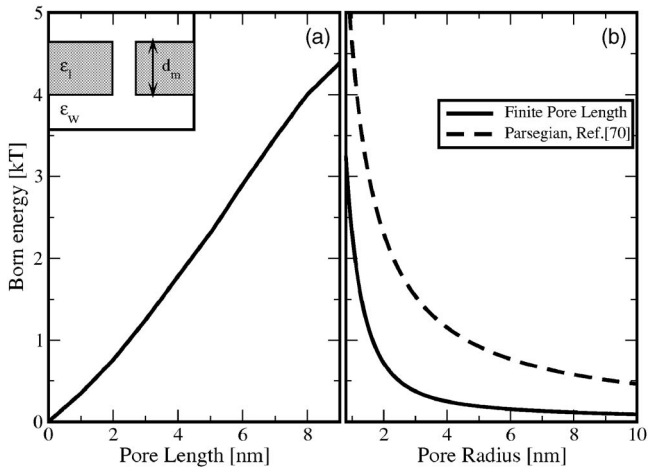

FIG. 5. The Born energy associated with ion partitioning into a membrane pore of cylindrical shape (shown in the inset) as function of (a) pore length (for a pore radius of $r_p = 1$ nm) and (b) pore radius (for a pore length of $d_m = 5$ nm). Finite-size membrane pores exhibit a substantial reduction of the Born energy in comparison with Parsegian's [70] infinite pore length results.

$$w_0(r_p) = \frac{1}{kT} \frac{(z_s e)^2}{4\pi\epsilon_l r_p} P\left(\frac{\epsilon_l}{\epsilon_w}\right) \frac{4\exp(-0.98 r_p) + 1}{5}. \tag{A7}$$

The rightmost factor of Eq. (A7) is an analytical fit to the numerically obtained electrostatic energy for the cylindrical pore-geometry shown in Fig. 5, and $P(\epsilon_l/\epsilon_w) = 0.17$ is a function of the lipid and electrolyte permittivities [69,70].

With $R_{spd}(r_p)$ and $R_{int}(r_p, r_s, U_m)$ in series the current through a single pore is

$$i_{p,s}(r_p, r_s) = \frac{1}{R_{spd} + R_{int}} U_m = \sigma_e \frac{A_{eff}(r_p, r_s, U_m)}{d_m} U_m, \tag{A8}$$

where we have introduced an effective area factor A_{eff},

$$A_{eff}(r_p, r_s, U_m) = \frac{A_p H(r_p, r_s) K(r_p, U_m)}{1 + \frac{A_p H(r_p, r_s) K(r_p, U_m)}{2 r_p d_m}}. \tag{A9}$$

Because the effective area is smaller than the membrane pore area, $A_{eff} < A_p = \pi r_p^2$, the main consequence of ion partitioning and hindrance is a reduction of the pore conductance with respect to the bulk electrolyte conductivity. As a consequence the pore conductance becomes a nonlinear (nonohmic) function of transmembrane voltage and depends both on the pore and ion radius.

Pores of different radii therefore have different contributions to the total membrane pore conductance $G_m^p(t)$, which is thus defined by the pore-size distribution $n(r_p,t)$. The total ionic conduction current through the membrane pores for ion species s is

$$\begin{aligned} I_{p,s}(t) &= \int i_{p,s} n(r_p,t) dr_p \\ &= \sigma_e \frac{U_m(t)}{d_m} \int A_{eff}(r_p,r_s) n(r_p,t) dr_p \\ &= G_{m,s}^p(t) U_m(t). \end{aligned} \tag{A10}$$

APPENDIX B: ATTEMPT RATE DENSITY AND LIPID FLUCTUATIONS

The microscopic picture behind the attempt rate density ν_0 was formulated, to our knowledge, for homogeneous defect nucleation in thin films (soap bubbles, fluid lipid membranes). However, it is also applicable to the dissipation of otherwise superfluid helium currents [71], and it is related to the fundamental frequency of atomic collisions per unit volume. We are interested here in the frequency of lateral lipid molecules fluctuations. A simple estimate can be obtained by treating the lateral fluctuations of the lipid heads in a bilayer leaflet as an ideal two-dimensional gas. A cutoff spatial displacement of the lipid molecules is $\Delta x = 0.15$ nm, above which water molecules are expected to start penetrating the membrane. Taking the molar mass of the lipid molecules to be approximately $M = 300$ g mol^{-1}, and using $M\langle v^2\rangle/2 = N_A kT$, we can estimate the time between collisions as $\Delta t = \Delta x/\sqrt{\langle v^2\rangle} = 1.2 \times 10^{-12}$ s. This picosecond time scale corresponds to approximately 800 collisions between the lipids in 1 ns, and a lipid fluctuation frequency of 8×10^{11} s^{-1}. It is within the upper end of the bandwidth of observed lipid fluctuation frequencies 10^7 s$^{-1} \leqslant \Delta\nu \leqslant 10^{12}$ s^{-1} [72].

By taking an average area of lipid heads of $A_{lip} = 0.6$ nm^2 [73] and assuming that a rearrangement of about 100 phospholipids are involved in the creation of a hydrophilic membrane pore, we estimate the attempt rate density to be

$$\nu_0 = \frac{1}{100 A_{lip} d_m \Delta t} = 3 \times 10^{36} \text{ m}^{-3} \text{ s}^{-1}. \tag{B1}$$

The main conclusions in this paper are not affected by whatever the effective value of ν_0 would be, as we extract the complete creation rate $\dot{N}_{c,min}$ from experimental data. However, as future MD simulation may be able to map out the complete free energy dispersion of membrane pores (and the crossover from hydrophobic to hydrophilic states) such that *ab initio* values for the pore creation energy δ_c and the pore destruction energy barrier δ_d can be obtained, it should be possible to infer the relevant value (or range of values) for ν_0 from the bandwidth of lipid fluctuation frequencies.

APPENDIX C: TRAPEZOIDAL PULSE TRANSMEMBRANE VOLTAGE DEPENDENCE

This section contains a collection of the definitions and abbreviations used in Sec. III C (and derived in Ref. [62]) to describe the initial course of the transmembrane voltage for an idealized trapezoidal electric pulse with rise time τ_{rise}. The functions K_1, K_2, and K_3 are given by

$$K_1 = \frac{a_1}{b_1},$$

$$K_2 = \frac{a_2}{2b_1} - \frac{a_1 b_2}{2b_1^2} + \frac{\frac{a_1 b_3}{b_1} + \frac{a_2 b_2}{2b_1} - \frac{a_1 b_2^2}{2b_1^2} - a_3}{\sqrt{b_2^2 - 4b_1 b_3}},$$

$$K_3 = \frac{a_2}{2b_1} - \frac{a_1 b_2}{2b_1^2} - \frac{\frac{a_1 b_3}{b_1} + \frac{a_2 b_2}{2b_1} - \frac{a_1 b_2^2}{2b_1^2} - a_3}{\sqrt{b_2^2 - 4b_1 b_3}}, \tag{C1}$$

in which the following constants are defined for the situation of identical internal and external electrolytes ($\sigma_{e,ex} = \sigma_{e,in} = \sigma_e$):

$$a_1 = 3d_m\sigma_e[\sigma_e(3r_{cell}^2 - 3d_m r_{cell} + d_m^2) + \sigma_m(3d_m r_{cell} - d_m^2)],$$

$$a_2 = 3d_m[2\sigma_e\epsilon_w(3r_{cell}^2 - 3d_m r_{cell} + d_m^2) + (\sigma_m\epsilon_w + \sigma_e\epsilon_l) \times (3d_m r_{cell} - d_m^2)],$$

$$a_3 = 3d_m\epsilon_w[\epsilon_w(3r_{cell}^2 - 3d_m r_{cell} + d_m^2) + \epsilon_l(3d_m r_{cell} - d_m^2)],$$

$$b_1 = 2r_{cell}^3(\sigma_m + 2\sigma_e)(\sigma_m + 0.5\sigma_e) - 2(r_{cell} - d_m)^3(\sigma_m - \sigma_e)^2,$$

$$b_2 = 2r_{cell}^3[\sigma_e(0.5\epsilon_l + \epsilon_w) + \sigma_m(2.5\epsilon_w + 2\epsilon_l) + \sigma_e(\epsilon_w + 2\epsilon_l)] + 2(r_{cell} - d_m)^3[2\sigma_e(\epsilon_l - \epsilon_w) + \sigma_m(\epsilon_w - 2\epsilon_l + \epsilon_w)],$$

$$b_3 = 2r_{cell}^3(\epsilon_l + 2\epsilon_w)(\epsilon_l + 0.5\epsilon_w) - 2(r_{cell} - d_m)^3(\epsilon_l - \epsilon_w)^2. \tag{C2}$$

Furthermore, the time constants

$$\tau_1 = \frac{2b_3}{b_2 - \sqrt{b_2^2 - 4b_1 b_3}},$$

$$\tau_2 = \frac{2b_3}{b_2 + \sqrt{b_2^2 - 4b_1 b_3}} \tag{C3}$$

correspond to the membrane charging time constant (τ_1) and the bulk electrolyte charging time constant (τ_2).

APPENDIX D: NANOSECOND PORE EXPANSION AND THE ASYMPTOTIC MODEL

Supraelectroporation leads to a huge number of membrane pores of minimum size. In particular, Fig. 4(e) shows that the mean pore radius hardly changes over the time scale

of the 10 ns pulse. Hence membrane pore creation dominates the electrical response and pore expansion is negligible. To make this statement more quantitative we consider the time immediately following the burst of pore creation. The transmembrane voltage plateaus at $U_m \approx 1$ V and the total pore energy ΔW for small pore radii 0.8 nm $< r_p <$ 1.5 nm is well approximated by a linear function in that limit:

$$\Delta W(r_p, U_m = 1\ \mathrm{V}) = -6.4 \times 10^{10} r_p kT\ \mathrm{m}^{-1}. \quad \text{(D1)}$$

The SE (2) then reduces to

$$\frac{\partial n}{\partial t} = D_p \frac{\partial^2 n}{\partial r_p^2} + v_d \frac{\partial n}{\partial r_p}, \quad \text{(D2)}$$

where the drift velocity is given by

$$v_d = \frac{D_p}{kT} \frac{\partial \Delta W(r_p)}{\partial r_p}. \quad \text{(D3)}$$

The pore distribution at the REB peak resembles a delta function at $r_{p,min}$, and the total number of pores does not change on a nanosecond time scale [see Fig. 4(c), following the burst of pore creation], so the normalized solution to Eq. (D2) is

$$n(r_p, t) = \frac{1}{\sqrt{4\pi D_p t}} \exp\left[-\frac{(r_p - r_{p,min} - v_d t)^2}{4 D_p t} \right]. \quad \text{(D4)}$$

The time-dependent mean pore radius is readily found from

$$\langle r_p(t) \rangle = \int n(r_p, t) r_p dr_p = r_{p,min} + v_d t. \quad \text{(D5)}$$

With the diffusion constant $D_p = 5 \times 10^{-14}$ m^2 s^{-1}, we find for the mean value of the pore radius $\langle r_p \rangle = 0.83$ nm after 10 ns. The corresponding single-pore conductances $G^p_{m,Cl^-}(r_p, U_m = 1\ \mathrm{V})$ at pore radii $r_p = 0.8$ nm and $r_p = 0.83$ nm differ by 10%. Taking this estimate as an analytical upper limit [the full simulation shows a smaller average pore radius, see Fig. 4(e)] for the magnitude of pore expansion we conclude that pore expansion is a negligible effect within the nanosecond time scale. This statement, however, depends on the value of the diffusion coefficient D_p for which only order of magnitude estimates exist so far. Bier *et al.* [74] derived an expression for D_p, which depends on the line tension γ and can be measured in principle, but results in even smaller values for D_p.

[1] K. H. Schoenbach, S. J. Beebe, and E. S. Buescher, Bioelectromagnetics (N.Y.) **22**, 440 (2001).
[2] S. J. Beebe, P. M. Fox, L. J. Rec, K. Somers, R. H. Stark, and K. H. Schoenbach, IEEE Trans. Plasma Sci. **30**, 286 (2002).
[3] S. J. Beebe, P. M. Fox, L. J. Rec, L. K. Willis, and K. H. Schoenbach, FASEB J. **17**, 1493 (2003).
[4] J. Deng, K. H. Schoenbach, E. S. Buescher, P. S. Hair, P. M. Fox, and S. J. Bebe, Biophys. J. **84**, 2709 (2003).
[5] P. T. Vernier, Y. Sun, L. Marcu, S. Salemi, C. M. Craft, and M. A. Gundersen, Biochem. Biophys. Res. Commun. **310**, 286 (2003).
[6] P. T. Vernier, L. I. Aimin, L. Marcu, C. M. Craft, and M. A. Gundersen, IEEE Trans. Dielectr. Electr. Insul. **10**, 795 (2003).
[7] P. T. Vernier, Y. Sun, L. Marcu, C. M. Craft, and M. A. Gundersen, Biophys. J. **86**, 4040 (2004).
[8] R. Nuccitelli, U. Pliquett, X. Chena, W. Forda, R. J. Swanson, S. J. Beebe, J. F. Kolb, and K. H. Schoenbach, Biochem. Biophys. Res. Commun. **343**, 351 (2006).
[9] D. A. Stewart, T. R. Gowrishankar, and J. C. Weaver, IEEE Trans. Plasma Sci. **32**, 1696 (2004).
[10] T. R. Gowrishankar, A. T. Esser, Z. Vasilkoski, K. C. Smith, and J. C. Weaver, Biochem. Biophys. Res. Commun. **341**, 1266 (2006).
[11] *Electroporation and Electrofusion in Cell Biology*, edited by E. Neumann, A. E. Sowers, and C. A. Jordan (Plenum Press, New York, 1989).
[12] *Guide to Electroporation and Electrofusion*, edited by D. C. Chang, B. M. Chassy, J. A. Saunders, and A. E. Sowers (Academic Press, New York, 1992).
[13] J. C. Weaver, J. Cell. Biochem. **51**, 426 (1993).
[14] J. C. Weaver and Y. A. Chizmadzhev, in *Handbook of Biological Effects of Electromagnetic Fields*, 2nd edition, edited by C. Polk and E. Postow (CRC Press, Boca Raton, 1996), pp. 247–274.
[15] *The Effects of High Intensity Electric Field Pulses on Eukaryotic Cell Membranes: Fundamentals and Applications*, edited by U. Zimmermann (CRC Press, Boca Raton, 1996).
[16] *Electrically Mediated Delivery of Molecules to Cells: Electrochemotherapy, Electrogenetherapy and Transdermal Delivery by Electroporation*, edited by M. J. Jaroszeski, R. Gilbert, and R. Heller (Humana Press, Totowa, 2000).
[17] J. C. Weaver, IEEE Trans. Dielectr. Electr. Insul. **10**, 754 (2003).
[18] K. H. Schoenbach, R. P. Joshi, J. R. Kolb, N. Chen, M. Stacey, P. F. Blackmore, E. S. Buescher, and S. J. Beebe, Proc. IEEE **92**, 1122 (2004).
[19] I. G. Abidor, V. B. Arakelyan, L. V. Chernomordik, Y. A. Chizmadzhev, V. F. Pastushenko, and M. R. Tarasevich, Bioelectrochem. Bioenerg. **6**, 37 (1979).
[20] V. F. Pastushenko, Y. A. Chizmadzhev, and V. B. Arakelyan, Bioelectrochem. Bioenerg. **6**, 53 (1979).
[21] Y. A. Chizmadzhev, V. B. Arakelyan, and V. F. Pastushenko, Bioelectrochem. Bioenerg. **6**, 63 (1979).
[22] V. F. Pastushenko, Y. A. Chizmadzhev, and V. B. Arakelyan, Bioelectrochem. Bioenerg. **6**, 71 (1979).
[23] V. B. Arakelyan, Y. A. Chizmadzhev, and V. F. Pastushenko, Bioelectrochem. Bioenerg. **6**, 81 (1979).
[24] V. F. Pastushenko, V. B. Arakelyan, and Y. A. Chizmadzhev, Bioelectrochem. Bioenerg. **6**, 89 (1979).
[25] V. F. Pastushenko, V. B. Arakelyan, and Y. A. Chizmadzhev, Bioelectrochem. Bioenerg. **6**, 97 (1979).
[26] L. V. Chernomordik, S. I. Sukharev, I. G. Abidor, and Y. A. Chizmadzhev, Bioelectrochem. Bioenerg. **9**, 149 (1982).
[27] V. F. Pastushenko and Y. A. Chizmadzhev, Gen. Physiol.

Biophys. **1**, 43 (1982).
[28] K. C. Melikov, V. A. Frolov, A. Shcherbakov, A. V. Samsonov, Y. A. Chizmadzhev, and L. V. Chernomordik, Biophys. J. **80**, 1829 (2001).
[29] J. C. Weaver and R. A. Mintzer, Phys. Lett. **86A**, 57 (1981).
[30] I. P. Sugar, J. Physiol. Paris **77**, 1035 (1981).
[31] K. T. Powell and J. C. Weaver, Bioelectrochem. Bioenerg. **15**, 211 (1986).
[32] R. Benz, F. Beckers, and U. Zimmermann, J. Membr. Biol. **48**, 181 (1979).
[33] A. Barnett and J. C. Weaver, Bioelectrochem. Bioenerg. **25**, 163 (1991).
[34] S. A. Freeman, M. A. Wang, and J. C. Weaver, Biophys. J. **67**, 42 (1994).
[35] R. P. Joshi and K. H. Schoenbach, Phys. Rev. E **62**, 1025 (2000).
[36] R. P. Joshi, Q. Hu, R. Aly, K. H. Schoenbach, and H. P. Hjalmarson, Phys. Rev. E **64**, 011913 (2001).
[37] R. P. Joshi, Q. Hu, K. H. Schoenbach, and H. P. Hjalmarson, Phys. Rev. E **65**, 041920 (2002).
[38] R. P. Joshi and K. H. Schoenbach, Phys. Rev. E **66**, 052901 (2002).
[39] R. P. Joshi, Q. Hu, K. H. Schoenbach, and S. J. Beebe, Phys. Rev. E **69**, 051901 (2004).
[40] Q. Hu, S. Viswanadham, R. P. Joshi, K. H. Schoenbach, S. J. Beebe, and P. F. Blackmore, Phys. Rev. E **71**, 031914 (2005).
[41] K. A. DeBruin and W. Krassowska, Ann. Biomed. Eng. **26**, 584 (1998).
[42] J. C. Neu and W. Krassowska, Phys. Rev. E **59**, 3471 (1999).
[43] K. A. DeBruin and W. Krassowska, Biophys. J. **77**, 1213 (1999).
[44] K. A. DeBruin and W. Krassowska, Biophys. J. **77**, 1225 (1999).
[45] A. O. Bilska, K. A. DeBruin, and W. Krassowska, Bioelectrochemistry **51**, 133 (2000).
[46] J. C. Neu, K. C. Smith, and W. Krassowska, Bioelectrochemistry **60**, 107 (2003).
[47] J. C. Neu and W. Krassowska, Phys. Rev. E **67**, 021915 (2003).
[48] K. C. Smith, J. C. Neu, and W. Krassowska, Biophys. J. **86**, 2813 (2004).
[49] D. P. Tieleman, H. Leontiadou, A. E. Mark, and S.-J. Marrink, J. Am. Chem. Soc. **125**, 6382 (2003).
[50] D. P. Tieleman, BMC Bioinf. **5**, 10 (2004).
[51] H. Leotiadou, A. E. Mark, and S. J. Marrink, Biophys. J. **86**, 2156 (2004).
[52] A. A. Gurtovenko and I. Vattulainen, J. Am. Chem. Soc. **127**, 17570 (2005).
[53] M. Tarek, Biophys. J. **88**, 4045 (2005).
[54] T. R. Gowrishankar and J. C. Weaver, Proc. Natl. Acad. Sci. U.S.A. **100**, 3203 (2003).
[55] D. A. Stewart, T. R. Gowrishankar, K. C. Smith, and J. C. Weaver, IEEE Trans. Biomed. Eng. **52**, 1643 (2005).
[56] M. Hibino, H. Itoh, and K. Kinosita, Biophys. J. **64**, 1789 (1993).
[57] J. C. Weaver and Y. A. Chizmadzhev, Bioelectrochem. Bioenerg. **41**, 135 (1996).
[58] B. V. Deryagin and Y. V. Gutop, Kolloidn. Zh. **24**, 370 (1962).
[59] R. W. Glaser, S. L. Leikin, L. V. Chernomordik, V. F. Pastushenko, and A. I. Sokirko, Biochim. Biophys. Acta **940**, 275 (1988).
[60] E. Evans, V. Heinrich, F. Ludwig, and W. Rawicz, Biophys. J. **85**, 2342 (2003).
[61] J. Darnell, H. Locish, and D. Baltimore, *Molecular Cell Biology* (Scientific American Books, New York, 1986).
[62] T. Kotnik, D. Miklavčič, and T. Slivnik, Bioelectrochem. Bioenerg. **45**, 3 (1998).
[63] W. Frey, J. A. White, R. O. Price, P. F. Blackmore, R. P. Joshi, R. Nuccitelli, S. J. Beebe, K. H. Schoenbach, and J. F. Kolb, Biophys. J. **90**, 3608 (2006).
[64] K. C. Smith, T. R. Gowrishankar, A. T. Esser, D. A. Stewart, and J. C. Weaver, IEEE Trans. Plasma Physics (to be published).
[65] W. Chen and R. C. Lee, Biophys. J. **67**, 603 (1994).
[66] W. Chen, Y. Han, Y. Chen, and D. Astumiam, Biophys. J. **75**, 196 (1998).
[67] J. Newman, J. Electrochem. Soc. **113**, 501 (1966).
[68] E. M. Renkin, J. Gen. Physiol. **38**, 225 (1954).
[69] V. A. Parsegian, Nature (London) **221**, 844 (1969).
[70] V. A. Parsegian, Ann. N.Y. Acad. Sci. **264**, 161 (1975).
[71] J. S. Langer and M. E. Fisher, Phys. Rev. Lett. **19**, 560 (1967).
[72] R. W. Glaser, Biochim. Biophys. Acta **940**, 275 (1988).
[73] J. Israelachvili, *Intermolecular and Surface Forces* (Academic Press, London, 1994).
[74] M. Bier, W. Chen, T. R. Gowrishankar, R. D. Astumian, and R. C. Lee, Phys. Rev. E **66**, 062905 (2002).
[75] J. Dai and M. P. Sheetz, Cold Spring Harb Symp. Quant Biol. **60**, 567 (1995).
[76] P. Läuger, *Electrogenic Ion Pumps* (Sinauer Associates, Sunderland, 1991).